Spatial and temporal evolution of the first-order phase transition in intrinsic optical bistability

Ramarao Inguva* and Charles M. Bowden
Research Directorate (AMSMI-RD-RE-OP), Research, Development, and Engineering Center, U.S. Army Missile Command, Redstone Arsenal, Alabama 35898-5248
(Received 7 April 1989)

Dynamical transient response and longitudinal spatial evolution of the first-order phase transition are presented for intrinsic optical bistability of a system of interacting spatially distributed, coherently driven two-level atoms. It is shown that a discontinuity in the nonlinear dielectric function is established internal to the medium due to transient response to a coherent, externally applied, time-dependent driving field, following the attainment of a critical value for the input intensity. If the externally applied field intensity reaches the steady state, beyond the critical value, the discontinuity of the nonlinear dielectric function in the medium reaches a stable stationary condition and forms a spatial boundary between states of high and low polarization in the medium. Thus it is shown that intrinsic optical bistability corresponds to a spatial as well as a temporal first-order phase transition in light-matter interactions, far from thermodynamic equilibrium, where the spatial boundary between different phases is established by transient dynamical response to the incident field.

I. INTRODUCTION

Intrinsic optical bistability[1] (IOB) is optical bistability[2] that does not depend upon optical or hybrid feedback. Experimental studies of IOB have been reported for a number of systems.[3,4] The origin of the different mechanisms has been interpreted as due to either thermal[3,5] or many-body interactions[4,6] of carriers in semiconductors. The universal characteristic for IOB in these systems is the existence of an intensity-dependent renormalization of the low-field intensity resonance, or gap frequency.

Since IOB is a genuine example of a first-order phase transition in a system of interacting light and matter, attention has been focused recently upon the theoretical analysis and interpretation of several fundamental prototype models.[7] The characterization of IOB for a system composed of a collection of laser field-driven nonlinear oscillators has been formulated.[8] Recently, this system has been analyzed in further detail in terms of longitudinal and transverse spatial effects and four-wave mixing.[9] Another model that has been analyzed in detail is that of an externally driven collection of spatially distributed, interacting, two-level atoms.[10] In the case of each model, under steady-state conditions, the existence and characteristics of a sharp discontinuity, in the propagation direction, of the nonlinear dielectric function in the material has been discussed.[9,11] The sharp boundary associated with the dielectric function is established in the medium for values of the externally applied field intensity which exceed the local IOB threshold at the input to the nonlinear material. It has been shown that the appearance of the discontinuity in the dielectric function can give rise to a significant backward propagating field amplitude, which together with the forward propagating field and the introduction of an incident probe field, results in four-wave mixing and phase-conjugate reflectivity.[9] Thus the phase-conjugate signal could be used to study the internal switching characteristics of the system.

The discontinuity in the nonlinear dielectric function in the direction of the propagation forms a spatial boundary between the regions of high- and low-polarization states of the material, and is unique to IOB [this phenomenon does not occur in systems that require optical feedback in a cavity to cause optical bistability (OB).] Indeed, the boundary spatially demarcates two regions in the material corresponding to the two separate phases of the first-order phase transition which coexist at the boundary, and thus characterizes IOB as a spatial, as well as temporal, first-order phase transition.

It is important to study the time dependence of the switching process and the dynamical buildup of the spatially dependent polarization and/or excitation in the nonlinear medium, which results in the spatial discontinuity in the dielectric function in the steady state discussed previously.[9–11] The purpose of this paper is to present an analysis and interpretation of the spatial and dynamical transient and temporal evolution to the steady state of the system of interacting, two-level atoms[10,11] upon switching in IOB.

In Sec. II, we present the modified Bloch-Maxwell equations derived previously,[10,11] and discuss the associated conditions for IOB. Also, we introduce the scaling procedure which is used to facilitate the spatial and temporal numerical integration, the results of which are presented and discussed in Sec. V. The slowly varying envelope approximation (SVEA) is discussed in relation to the modified Bloch-Maxwell equations in Sec. III and, in Sec. IV, its degree of validity in the treatment presented here is discussed in relation to the second-order

Maxwell wave equation in the steady state. The dynamics of the spatially dependent switching process is presented in Sec. V in the SVEA. The final section is used for a summary of results and conclusions.

II. TIME-DEPENDENT EQUATIONS FOR A TWO-LEVEL SYSTEM

We consider here a system composed of spatially extended, interacting, two-level atoms driven by an externally applied electromagnetic field at a frequency ω. We neglect here any transverse effects. The equations of motion derived earlier by Ben-Aryeh *et al.*[1] are given by

$$\frac{d\langle\sigma_z\rangle}{dt}=-\gamma_L(1+\langle\sigma_z\rangle)+\frac{\mu}{\hbar}(E^*\langle\sigma_+\rangle+E\langle\sigma_-\rangle)\ , \tag{1}$$

$$\frac{d}{dt}\langle\sigma_+\rangle=-\frac{\mu E}{2\hbar}\langle\sigma_z\rangle-[\gamma_T-i(\Delta-\epsilon\langle\sigma_z\rangle)]\langle\sigma_+\rangle\ , \tag{2}$$

$$\langle\sigma_-\rangle=\langle\sigma_+\rangle^*\ , \tag{3}$$

$$\left[\frac{\partial^2E}{\partial z^2}+\frac{\omega^2E}{c^2}\right]+\frac{2i\omega}{c^2}\frac{\partial E}{\partial t}=-i\frac{8\pi n\omega^2}{c^2}\langle\sigma_+\rangle\ . \tag{4}$$

In Eqs. (1)–(4), $\langle\sigma_z\rangle$ is the average atomic inversion per unit volume, $\langle\sigma_+\rangle$ is the average complex atomic polarization per unit volume, and E is the positive frequency part of the temporally slowly varying envelope of the electric field [the slowly varying envelope approximation in time has already been used in deriving Eqs. (1)–(4)]. The parameter μ in Eqs. (1) and (2) is the absolute value of the transition dipole moment matrix element of each identical atom in the system. ω is the frequency of the incident field and n is the number density of atoms. The rates γ_L and γ_T are the inverses of the population relaxation time T_1 and the dipole relaxation time T_2, respectively. The detuning parameter Δ is given by $(\omega-\omega_0)$ and is the deviation of the applied field frequency from the atomic resonance frequency ω_0. The quantity ϵ in Eqs. (1)–(3) is the frequency renormalization constant caused by near dipole-dipole interaction in a dense medium[1] given by

$$\epsilon=\frac{7\pi n\beta c^3}{4\omega_0^3}\ , \tag{5}$$

where β is the spontaneous decay rate which has the value

$$\beta=\frac{4|\mu|^2\omega_0^3}{3\hbar c^3}\ . \tag{6}$$

In a fully quantum-mechanical model γ_L and γ_T are given in terms of β by

$$\gamma_L=\beta,\quad \gamma_T=\tfrac{1}{2}\beta\ . \tag{7}$$

The usual Maxwell-Bloch equations for gases or tenuous media are recovered by setting the constant ϵ to zero.

Before we begin our analysis it is useful and instructive to recast Eqs. (1)–(4) in dimensionless form by introducing the following set of scaled variables and parameters:

$$\begin{aligned}
&\bar{E}=\frac{\mu E}{\hbar\gamma_L}\ ,\\
&\bar{I}=|\bar{E}|^2\ ,\\
&\bar{\Delta}=\frac{\Delta}{\gamma_L}\ ,\\
&\bar{\epsilon}=\frac{\epsilon}{\gamma_L}=(\tfrac{7}{32}\pi^2)n\lambda_0^3\ ,\\
&w=\langle\sigma_z\rangle,\quad p_\pm=\langle\sigma_\pm\rangle\ ,\\
&s_0=\frac{4\pi n\mu^2\omega}{\hbar c},\quad z_0=\frac{\gamma_L}{s_0}=\frac{\omega}{\omega_0}\left[\frac{3n\lambda_0^2}{4\pi}\right]\ ,\\
&\bar{t}=\gamma_L t,\quad \bar{z}=\frac{z}{z_0}\ ,\\
&k_0=\frac{2\pi}{\lambda_0}=\frac{\omega_0}{c},\quad \bar{k}=k\left[\frac{\gamma_L}{s_0}\right]=\left[\frac{8\pi^2}{3n\lambda_0^3}\right]\ .
\end{aligned} \tag{8}$$

In terms of these new quantities, Eqs. (1)–(4) can be rewritten as

$$\frac{dw}{dt}=-(1+w)+\bar{E}^*p_++\bar{E}p_-\ , \tag{9}$$

$$\frac{d}{dt}p_+=-\tfrac{1}{2}\bar{E}w-[\bar{\gamma}_T-i(\bar{\Delta}-\bar{\epsilon}w)]p_+\ , \tag{10}$$

$$\left[\frac{\partial^2\bar{E}}{\partial\bar{z}^2}+\bar{k}^2\bar{E}\right]+2i\bar{k}\eta\frac{\partial E}{\partial\bar{t}}=-2i\bar{k}p_+\ , \tag{11}$$

$$\eta=\gamma_L^2/cs_0\ . \tag{12}$$

The quantity $\bar{k}$ can be thought of as an effective wave number and it depends on the density and the resonance wavelength via the parameter $n\lambda_0^3$. Equations (9)–(12) are the starting point for the analysis to be presented in the remainder of this paper.

Under steady-state conditions we obtain the following equations for the polarization, inversion, and the field variables (obtained by setting all time derivatives equal to zero),

$$p_s=-\tfrac{1}{2}\bar{E}_s\frac{w_s}{\bar{\gamma}_T-i(\bar{\Delta}-\bar{\epsilon}w_s)}\ , \tag{13}$$

$$(1+w_s)[\bar{\gamma}_T^2+(\bar{\Delta}-\bar{\epsilon}w)^2]=-\bar{I}w_s\bar{\gamma}_T\ , \tag{14}$$

$$\frac{d^2\bar{E}_s}{d\bar{z}^2}+q^2(\bar{z})\bar{E}_s=0\ , \tag{15}$$

$$q^2(\bar{z})=\bar{k}^2-i\bar{k}w_s[\bar{\gamma}_T-i(\bar{\Delta}-\bar{\epsilon}w_s)]^{-1}\ . \tag{16}$$

In Eqs. (13)–(16) we have labeled all steady-state values by the subscript s. We note that the field equation is nonlinear since q^2 depends on w which in turn is coupled to p and $\bar{E}$. We will return to a discussion of the steady state in Sec. IV.

III. SLOWLY VARYING ENVELOPE APPROXIMATION

The time-dependent, nonlinear coupled equations (9)–(12) for inversion w, polarization p, and field $\bar{E}$ are, in general, difficult to solve even numerically. In this section we study the application of the standard slowly varying envelope approximation for the spatial dependence to simplify the equations. In Sec. IV we will address the question of the validity of the SVEA for the steady state.

We begin by decomposing the inversion, polarization, and the field variables into forward and backward propagating parts,

$$\bar{E}^{+}=E_F^{+}e^{i\bar{k}\bar{z}}+E_B^{+}e^{-i\bar{k}\bar{z}}\ , \tag{17}$$

$$p_{+}=p_F^{+}\exp(i\bar{k}\bar{z})+p_B^{+}\exp(-i\bar{k}\bar{z})\ , \tag{18}$$

$$w=w_0+w_1\exp(2i\bar{k}\bar{z})+w_1^{*}\exp(-2i\bar{k}\bar{z})\ , \tag{19}$$

$$p_{-}=p_{+}^{*}\ . \tag{20}$$

In SVEA we treat the variables E_F, E_B, p_B, w_0, w_1, and p_F as slowly varying and neglect all second and higher derivatives of these quantities. In Eqs. (17)–(20) we have introduced the superscripts + explicitly to indicate positive frequency parts. Substituting Eqs. (17)–(20) into Eqs. (9)–(12) and keeping only the leading spatial frequency terms [in powers of $\exp(ikz)$ and $\exp(-ikz)$], we obtain the following equations for inversion, polarization, and fields:

$$\frac{dw_0}{d\bar{t}}=-(1+w_0)+E_F^{-}p_F^{+}+E_B^{-}p_B^{+}+E_F^{+}p_F^{-}+E_B^{+}p_B^{-}\ , \tag{21}$$

$$\frac{dw_1}{d\bar{t}}=-w_1+p_B^{-}E_F^{+}+p_F^{+}E_B^{-}\ , \tag{22}$$

$$\frac{dp_F^{+}}{d\bar{t}}=-\tfrac{1}{2}(w_0E_F^{+}+w_1E_B^{+})-[\bar{\gamma}_T-i(\bar{\Delta}-\bar{\epsilon}w_0)]p_F^{+}-i\epsilon w_1p_B^{+}\ , \tag{23}$$

$$\frac{d}{d\bar{t}}p_B^{+}=-\tfrac{1}{2}(w_0E_B^{+}+w_1^{*}E_F^{+})-[\bar{\gamma}_T-i(\bar{\Delta}-\bar{\epsilon}w_0)]p_B^{+}-i\epsilon w_1^{*}p_F^{+}\ , \tag{24}$$

$$\eta\frac{\partial E_F^{+}}{\partial\bar{t}}+\frac{\partial E_F^{+}}{\partial\bar{z}}=-p_F^{+}\ , \tag{25}$$

$$\eta\frac{\partial E_B^{+}}{\partial\bar{t}}-\frac{\partial E_B^{+}}{\partial\bar{z}}=-p_B^{+}\ , \tag{26}$$

and the intensity $\bar{I}$ is defined by

$$\bar{I}=|E_F^{+}|^2+|E_B^{+}|^2+E_F^{+}E_B^{+*}e^{2i\bar{k}\bar{z}}+E_B^{+}E_F^{+*}e^{-2i\bar{k}\bar{z}}\ . \tag{27}$$

In the special case when the backward wave contributions can be dropped the above equations reduce to the following simplified set (obtained by setting p_B, E_B to zero):

$$\frac{dw_0}{d\bar{t}}\cong-(1+w_0)+E_F^{-}p_F^{+}+E_F^{+}p_F^{-}\ , \tag{28}$$

$$\frac{dw_1}{d\bar{t}}\cong-w_1\ , \tag{29}$$

$$\frac{dp_F^{+}}{d\bar{t}}=-\tfrac{1}{2}w_0E_F^{+}-[\bar{\gamma}_T-i(\bar{\Delta}-\bar{\epsilon}w_0)]p_F^{+}\ ,$$

$$\eta\frac{\partial E_F^{+}}{\partial\bar{t}}+\frac{\partial E_F^{+}}{\partial\bar{z}}=-p_F^{+}\ , \tag{30}$$

$$\bar{I}=|E_F^{+}|^2\ .$$

Under steady-state conditions, Eqs. (28)–(30) become

$$p_s=-\frac{(E_sw_s/2)}{[\bar{\gamma}_T-i(\bar{\Delta}-\bar{\epsilon}w_s)]}\ ,$$

$$(1+w_s)[\bar{\gamma}_T^{\,2}+(\bar{\Delta}-\bar{\epsilon}w_s)^2]=-\bar{I}_sw_s\bar{\gamma}_T\ , \tag{31}$$

$$\frac{\partial\bar{I}_s}{\partial\bar{z}}=-(1+w_s)\ ,$$

where we indicated all steady-state values by the subscript s. This set of coupled equations was analyzed earlier by Ben-Aryeh *et al.*,[1] who showed the existence of a spatial first-order phase transition characterized by a spatial discontinuity in inversion from a value of $w\lesssim 0$ to a value of -1 and also a kink in the intensity as a function of z for all values of $\bar{\epsilon}>3$ and intensities greater than a threshold value. These authors suggested that this phase transition caused by nonlinear atomic frequency renormalization in intrinsic optical bistability may be observable in systems characterized by high density and high oscillator strengths.

The validity of the SVEA and the neglect of the backward wave contributions have not been investigated earlier. In Sec. IV we address this question in some detail and show that the SVEA is a reasonable approximation, even though the reasons for its validity are different from the usual ones suggested in the literature. The time-dependent equations are then studied in the SVEA in Sec. V to obtain switching times and dynamical transient effects related to the time dependence of evolution in intrinsic optical bistability.

IV. STEADY STATE AND DEGREE OF VALIDITY OF THE SVEA

In this section we study the behavior of the two-level system under steady-state conditions. We solve Eqs. (13)–(16) using second-order field equations as well as the approximate set (31) using the SVEA and compare the two.

Because of their nonlinear nature, the solution of the coupled equations for inversion, polarization, and fields can only be achieved numerically and we outline our procedure here. Consider the two-level system confined to a one-dimensional box of length L (the transverse effects have been neglected). The electric field, being incident from the left, is assumed as given for all time at $z=0$. The system outside the sample of length L is assumed to be a vacuum. The fields outside are then of the form

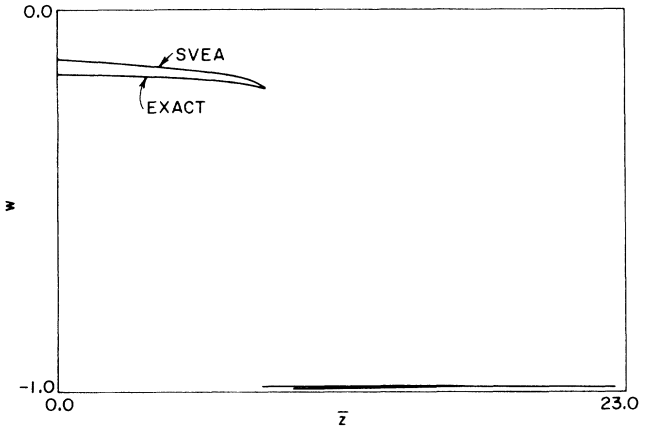

FIG. 1. Plot of the inversion $w(\bar{z})$ as a function of $\bar{z}$ for the parameters $\bar{\epsilon}=10$, $\bar{\Delta}=-2$, $\bar{\gamma}_T=0.5$, $E_I=3.0$, and sample length $\bar{L}=22.5$.

$$\begin{aligned}\bar{E}(\bar{z})&=E_I(e^{ik\bar{z}}+re^{-ik\bar{z}}), \quad z<0\\ &=E_Te^{ik\bar{z}}+E_Re^{-ik\bar{z}}, \quad z>L\end{aligned} \tag{32}$$

where E_I is the incident field and rE_I is the reflected field amplitude (the coefficient r is unknown). E_T is the amplitude of the transmitted field. The coefficients r, E_T, and E_R are unknown and have to be determined self consistently so as to match the solution inside the medium. Since the system is not confined to a cavity, the coefficient E_R must have the value

$$E_R=0\ . \tag{33}$$

This situation does not arise for the SVEA which has only first-order derivatives and hence the specification of the incident field is sufficient [see Eqs. (28)–(30)].

Our procedure for solving the second-order field equations is as follows. We assume that w is a smooth function of z except for possible jump discontinuities. We then divide the space $0<z<L$ into n subregions in each of which w is assumed to be constant. The quantity $q^2(z)$ in the jth region is then constant and the field in the jth region can be written as

$$\bar{E}=C_je^{iq_j(z-z_{j-1})}+D_je^{-iq_j(z-z_{j-1})}, \quad z_{j-1}<z<z_j \tag{34}$$

where the coefficients C_j, D_{j-1} have to be determined using the boundary conditions, namely, the continuity of the field and its first derivative at each boundary ($z=0, z_1, z_2, z_3, \ldots, z_n$). The unknowns E_T and E_R can be related to E_I and r by

$$\begin{bmatrix}E_T\\ E_R\end{bmatrix}=U\begin{bmatrix}E_I\\ rE_I\end{bmatrix}, \tag{35}$$

where the matrix U is given by (h is the width of any region)

$$U=U_0U_1U_2U_3\cdots U_{N-1}U_N\ , \tag{36}$$

$$U_0=\begin{bmatrix}\frac{1}{2}(1+\bar{k}/q_1) & \frac{1}{2}(1-k/q_1)\\ \frac{1}{2}(1-\bar{k}/q_1) & \frac{1}{2}(1+k/q_1)\end{bmatrix}, \tag{37}$$

$$U_N=\begin{bmatrix}\frac{1}{2}\left[1+\frac{q_N}{\bar{k}}\right]e^{iq_Nh} & \frac{1}{2}\left[1-\frac{q_N}{k}\right]e^{-iq_Nh}\\ \frac{1}{2}\left[1-\frac{q_N}{\bar{k}}\right]e^{+iq_Nh} & \frac{1}{2}\left[1+\frac{q_N}{k}\right]e^{iq_Nh}\end{bmatrix}, \tag{38}$$

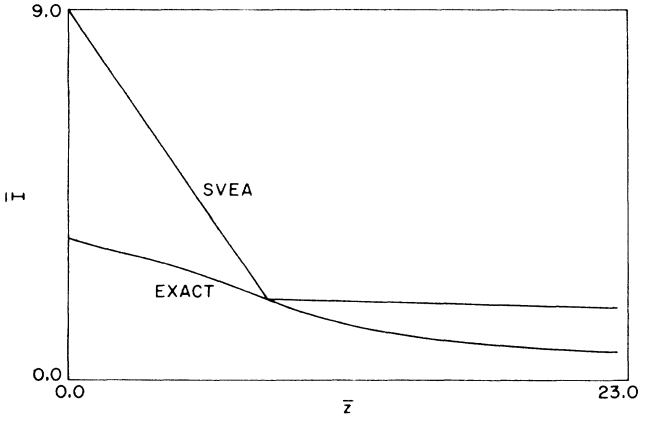

FIG. 2. Plot of intensity (dimensionless) $\bar{I}$ as a function of $\bar{z}$ for the same parameters as in Fig. 1.

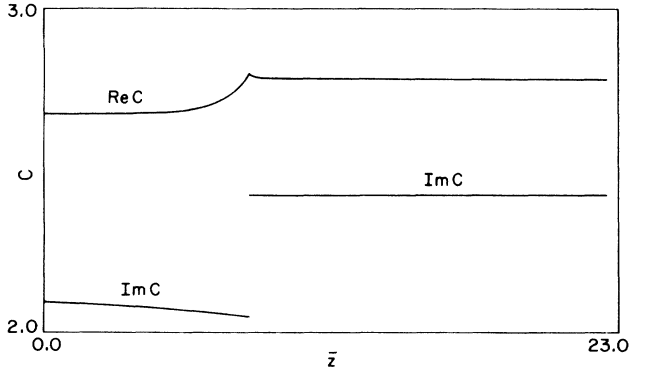

FIG. 3. Plot of the complex coefficient C as a function of $\bar{z}$ [see Eq. (34)].

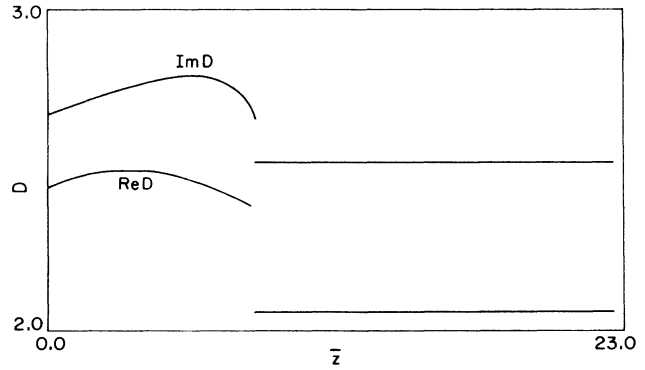

FIG. 4. Plot of the complex coefficient D of Eq. (34) as a function of $\bar{z}$. The parameters are the same as in Fig. 1.

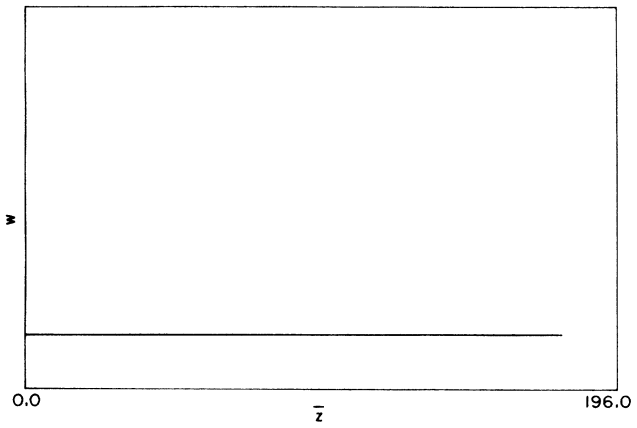

FIG. 5. Plot of $w(z)$ as a function of $\bar{z}$ at time $\bar{t}=1$ for parameters $\bar{\Delta}=-2$, $\bar{\epsilon}=10$, $\bar{\gamma}=0.5$, $\eta=0.001$.

$$U_j=\begin{bmatrix} \frac{1}{2}(1+q_j/q_{j+1})e^{iq_jh} & \frac{1}{2}(1-q_j/q_{j+1})e^{-iq_jh} \\ \frac{1}{2}(1-q_j/q_{j+1})e^{iq_jh} & \frac{1}{2}(1+q_j/q_{j+1})e^{-iq_jh} \end{bmatrix} . \tag{39}$$

The numerical calculation for the determination of r proceeds as follows: we start with an initial guess for the complex quantity r and solve for E_T and E_R. Since there is no reflected component in region $z>L$ we set E_R to zero to obtain the condition

$$E_R=E_I(U_{21}+rU_{22})=0 ,$$
$$r=-\frac{U_{21}}{U_{22}} . \tag{40}$$

The resulting output value for r is then used as the next trial value for r until the vanishing of E_R is satisfied to a specified accuracy. In practice, to ensure convergence, we use the average of the input and output values of r as the next value for r. We have used the condition $|E_R/E_I|\leq 0.0001$ for the determination of r. The results for the model set of parameters $\bar{\epsilon}=10.0$, $\Delta=-2.0$, $\bar{\gamma}_T=0.5$, $E_I=3.0$, and $L=22.5$ are shown in Figs. 1 and 2 for the inversion and the intensity. In these figures we also show the SVEA results for the same set of parameters. We note that the results for the inversion are quite close. The earlier prediction of the occurrence of the boundary separating the two regions $w\lesssim 0$ and $w\geq -1$ is therefore not an artifact of the SVEA but is indeed borne out by the full second-order calculation of the field. The results for the intensity do show some differences of the order of 5–20%, depending on the choice of model parameters. Most of the difference can be attributed to the neglect of the backward wave contributions neglected in the simplified set of equations (28)–(30). To see this aspect we plot in Figs. 3 and 4 the real and imaginary parts of C_j and D_j. We note from these figures that C and D are approximately constant except in the region of discontinuity. This in turn implies that

$$\frac{d^2C}{d\bar{z}^2}=0, \quad \frac{d^2D}{d\bar{z}^2}=0 , \tag{41}$$

which in fact is at the heart of the SVEA. In the upper region (characterized by $w\lesssim 0$) $q^2(z)$ takes the value

$$q^2\simeq \bar{k}^2 .$$

Thus the SVEA is expected to be accurate in the region where $w\lesssim 0$. In the region to the right of the boundary the intensity is attenuated, Beer's law is approximately satisfied, and the differences between the SVEA and the second-order results are minor. Thus, even though the sample size is not large compared to a wavelength at

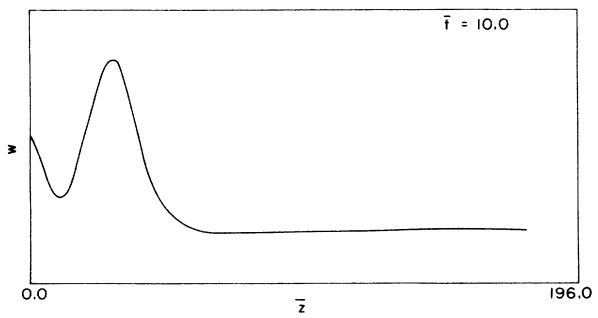

FIG. 6. Same as Fig. 5 except $\bar{t}=10$.

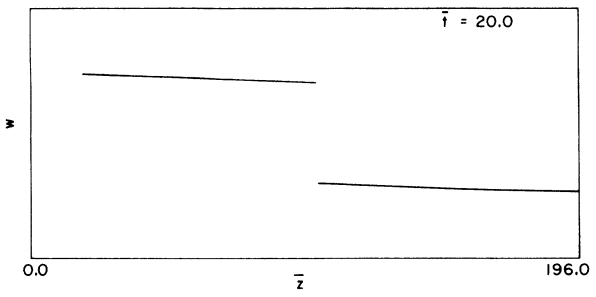

FIG. 7. Same as Fig. 6 except $\bar{t}=20$.

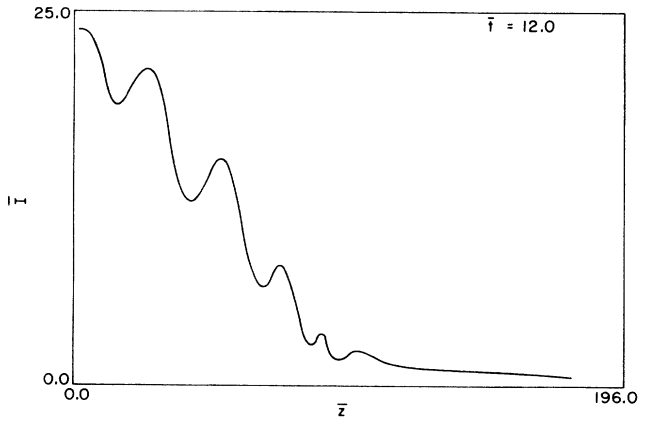

FIG. 8. Plot of dimensionless intensity $\bar{I}$ at time $\bar{t}=12$. The parameters are the same as in Fig. 5.

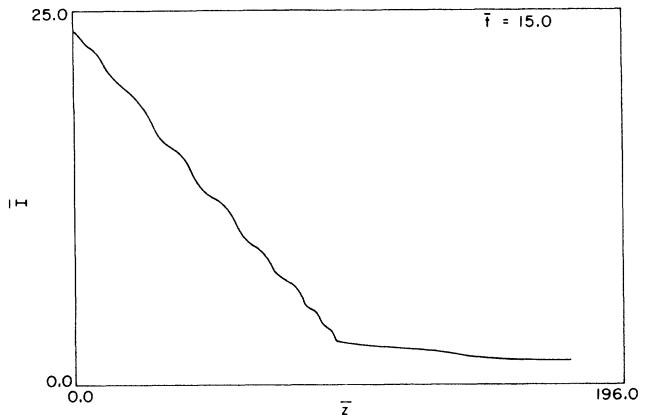

FIG. 9. Same as Fig. 8 except that $\bar{t}=15$.

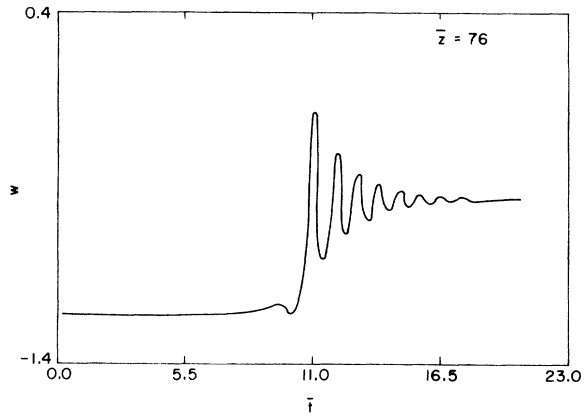

FIG. 11. Plot of inversion w as a function of dimensionless time at a distance $\bar{z}=76$. The parameters are the same as in Fig. 5.

which the medium exhibits bistability, the SVEA is nevertheless satisfied due to the feature that w is slowly varying in each phase. This gives us confidence in using the SVEA for analyzing the time-dependent equations. We turn to the time-dependent problem in Sec. V.

V. TEMPORAL EVOLUTION OF INTRINSIC OPTICAL BISTABILITY IN THE SVEA

In this section we analyze the time-dependent equations in the SVEA (i.e., the SVEA for both time and spatial coordinates). We note from the discussion at the end of Sec. IV that the reflection coefficient $R=|r|^2$ is small, of the order of 0.2 or less. To keep the analysis simple we set $r=0$ and neglect the backward wave contributions altogether. The resulting set of equations has been given in Sec. III [see Eqs. (28)–(30)]. Thus we have to solve a set of coupled first-order partial differential equations for the inversion w, the polarization P_F, and the field E_F.

We use the numerical method adopted earlier by Fleck.[12] For a specified incident field E at $z=0$ and initial values for w_0, w_1, and P_F at $t=0$, we solve[12] for the time dependence at various spatial grid points $0<z<L$ in the sample. The step size Δz for z is determined by

$$\Delta z=\Delta t/\eta\ ,$$

and hence is controlled by the value of η. In practice, for a given value of η a choice is made for Δt so as to give a reasonable choice for Δz. The smaller the value of η the larger the number of time steps to achieve a given step size of z, say unity, and this in turn increases the computational time. We have chosen the representative value of $\eta=0.001$ for the calculations presented in this section. The results do not exhibit a strong variation as η is decreased.

In Figs. 5–7 we show the spatial variation of w for times $\bar{t}=1$, 10, and 20 for input parameters $\Delta=-2$, $\bar{\epsilon}=10.0$, $\bar{\gamma}=0.5$, and $\eta=0.001$. The parameters are chosen to be the same as those used earlier by Ben-Aryeh *et al.*[11] The time scale is in units of γ_L^{-1}. We find that it takes typically a few γ_L^{-1} in time for the system to switch to the state characterized by $w\lesssim 0$ starting from an initial state of $w=-1$. The emergence of a nonlinear dielectric boundary is clearly seen in Fig. 7 at $\bar{z}=94$. The steady-state values for w are in reasonable agreement with the earlier work of Ben-Aryeh *et al.*[1,11] In Figs. 8–10, we plot the intensity at $\bar{t}=12$, 15, and 20. Again we see the emergence of a sharp boundary separating the two phases in the medium by the presence of a kink at $\bar{z}=94$. Next

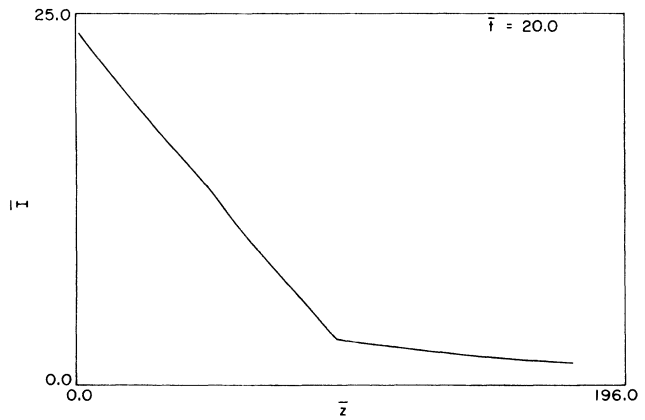

FIG. 10. Same as Fig. 8 except that $\bar{t}=20$.

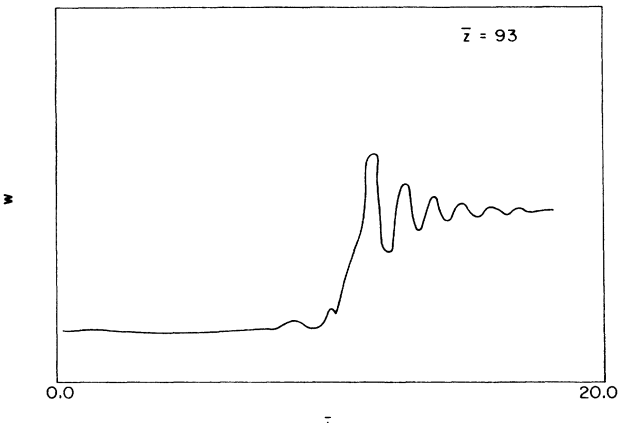

FIG. 12. Same as Fig. 11 except $\bar{z}=93$.

we study the time dependence of w as a function of time at various spatial locations. In Figs. 11–13 we exhibit the time dependence of w at locations $\bar{z}=76$, 93, and 94. The approach to the steady state is clearly seen in these figures and takes approximately $10\gamma_L^{-1}-15\gamma_L^{-1}$ depending on the spatial location (hence the intensity value). We note from Figs. 11–13 that the switching time increases dramatically at the discontinuity as $z=94$ is approached. The figure for $\bar{z}=94$ (Fig. 13) shows that at the boundary it takes much longer for the system to settle into the upper state characterized by the lower absorption ($w\cong 0$). This is due to the well-known critical slowing-down phenomenon.

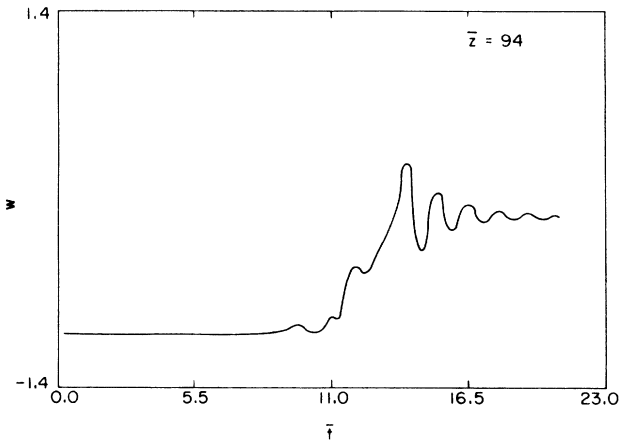

FIG. 13. Same as Fig. 11 except $\bar{z}=94$.

VI. CONCLUSION

We have used the modified Maxwell-Bloch formulation derived previously[10,11] to analyze the dynamics and spatial dependence of the switching process in IOB. The results, in the steady state using the SVEA, were compared with the corresponding results using the second-order Maxwell equation in the propagation spatial variable (SVEA in time only), and the comparison is quite good for our case, as shown in Fig. 1. The equations in the SVEA were integrated temporally and spatially, using a step-function input pulse of intensity above threshold, and the dynamical evolution of the nonlinear dielectric function spatial discontinuity is depicted in Figs. 11–13. The dielectric boundary is established in the medium, through transient evolution, corresponding to the point z at which the local intensity I is at the lower bistable threshold. The boundary occurs as a limiting steady-state condition through the dynamical transients of the switching process. Critical slowing down is indicated in Figs. 11–13 as z approaches the critical value in the medium. Different shaped pulses will cause different fluctuation and oscillation patterns in the transient response, but the steady state will always be the same. The use of four-wave mixing could be used to monitor and study the fluctuations and oscillations associated with the spatial and temporal buildup of the internal boundary between the two states of polarization.[9] The emergence of the backward wave is a reflection of the presence of the internal boundary induced by the highly nonlinear interaction of the laser beam with the system. No additional scattering effects are expected in the present framework. We feel that this feature of IOB is of sufficient fundamental interest to warrant further theoretical as well as experimental investigation.

ACKNOWLEDGMENTS

R.I. acknowledges support from the National Research Council.

*On leave from the University of Wyoming.

[1]Y. Ben-Aryeh, C. M. Bowden, and J. C. Englund, Phys. Rev. A **34**, 3917 (1986); B. Ritchie and C. M. Bowden, *ibid.* **32**, 2293 (1985); C. M. Bowden, in *Quantum Optics IV*, edited by D. F. Walls and J. D. Harvey (Springer, Berlin, 1986), p. 139, and references therein.

[2]L. A. Lugiato, in *Progress in Optics XXI*, edited by E. Wolf (North-Holland, Amsterdam, 1964), p. 89.

[3]J. Hajto and I. Janossy, Philos. Mag. B **47**, 347 (1983); D. A. B. Miller, A. C. Gossard, and W. Wiegmann, Opt. Lett. **9**, 162 (1984); M. Dagenais and W. Z. Sharfin, Appl. Phys. Lett. **45**, 210 (1984).

[4]K. Bohnert, H. Kalt, and C. Klingshirn, Appl. Phys. **43**, 1088 (1983); H. Rossmann, F. Henneberger, and H. Voigt, Phys. Status Solidi B **115**, K63 (1983); F. Henneberger and H. Rossmann, *ibid.* **121**, 685 (1984).

[5]C. M. Bowden, C. C. Sung, J. W. Haus, and J. M. Cook, J. Opt. Soc. Am. B **3**, 1206 (1986).

[6]H. E. Schmidt, H. Haug, and S. W. Koch, Appl. Phys. Lett. **44**, 787 (1984).

[7]C. M. Bowden, in *Quantum Optics IV*, Vol. 12 of Springer Proceedings in Physics, edited by J. D. Harvey and D. F. Walls (Springer-Verlag, New York, 1986), p. 139.

[8]J. A. Goldstone and E. Garmire, Phys. Rev. Lett. **53**, 910 (1984); C. Flytzanis and C. S. Tang, *ibid.* **45**, 441 (1980); B. Ritchie and C. M. Bowden, Phys. Rev. A **32**, 2293 (1985); E. Liu and J.-M. Yuan, *ibid.* **29**, 2257 (1984).

[9]J. W. Haus, Li Wang, M. Scalora, and C. M. Bowden, Phys. Rev. A **38**, 4043 (1988).

[10]Y. Ben-Aryeh, C. M. Bowden, and J. C. Englund, Phys. Rev. A **34**, 3917 (1986), and references therein.

[11]Y. Ben-Aryeh, C. M. Bowden, and J. C. Englund, Opt. Commun. **61**, 147 (1987).

[12]J. A. Fleck, Jr., Phys. Rev. B **1**, 84 (1970).